Raman scattering study of lattice disorder in 1-MeV Si-implanted GaAs

G. Braunstein, D. Tuschel,[a] Samuel Chen, and S.-Tong Lee
Corporate Research Laboratories, Eastman Kodak Company, Rochester, New York 14650

(Received 1 May 1989; accepted for publication 5 July 1989)

We have used Raman scattering to study the lattice disorder created by the implantation of 1-MeV Si ions into GaAs. Using the change in the longitudinal optical (LO) phonon-line position as the signature for lattice damage, combined with chemical etching for controlled layer removal, we monitored the evolution of the disorder depth profile as a function of implantation dose. The shape of the depth profile of the disorder agrees with the theoretical simulation TRIM for doses of 1×10^{14} cm^{-2} or lower. For higher doses a saturation is observed in the amount of residual disorder. This saturation is a manifestation of dynamic annealing occurring during the high-energy implantations, which we attribute to enhanced defect mobility, induced by the transfer of energy to the lattice, in atomic collision cascade processes. In order to correlate the spectral features in the Raman spectra with structural changes in the ion-implanted samples, we characterized the implantation-induced lattice damage using ion-channeling and transmission electron microscopy (TEM) measurements. The residual defects in the MeV-implanted samples are found to consist of dislocation loops and discrete point defects dispersed in an otherwise perfect (although probably strained) crystalline lattice. An average distance between defects was estimated from the channeling and TEM studies, and compared with the coherence-length parameter L used in the "spatial correlation model," which is commonly used to interpret quantitatively the Raman spectra of ion-implanted materials. Although the model gives a good fit to our data in terms of the position and linewidth of the LO phonon peak, no clear correlation could be established between L and the interdefect separations. We also observed the appearance of the broadbands at about 70, 180, and 245 cm^{-1}, in the Raman spectra, which are commonly attributed to amorphous GaAs, although no trace of amorphous material was detected by the TEM analysis. Our results indicate that the quantitative interpretation of Raman spectra to determine crystalline properties of ion-implanted materials, as well as the assignment of Raman spectral features to particular defect structures, is not unambiguously established yet.

I. INTRODUCTION

Ion implantation at 30–200 keV (low-energy implantation in the context of the present work) is a well-established processing step in the semiconductor industry.[1] With the advent of more reliable high-energy ion implanters, it becomes possible to extend the range of applicability of this technology into the megavolt (MeV) energy regime, thus providing device designers with increased possibilities for the development of novel device structures.[2] The optimization of the new process requires, as was the case with the low-energy implantations, a detailed characterization of the lattice disorder created by the implanted ions. Such characterization can be accomplished using one or more of several different experimental techniques like ion channeling, transmission electron microscopy (TEM), electronic transport measurements, optical spectroscopy, etc.[3] Among the optical measurements, Raman scattering has emerged as a very useful characterization tool to evaluate the structural properties of ion-implanted materials. Lattice defects and structural changes induce significant modifications to the Raman spectrum of a material, which allow monitoring of the evolution of the radiation damage.[4–6] In addition, Raman scattering experiments in opaque semiconductors probe the near-surface region to depths of the order of thousand angstroms, nearly the same magnitude as the penetration depth of the ions in a typical low-energy implantation. When the energy of the implants is in the MeV range, implantation effects can extend several micrometers deep into the sample. In this case a combination of Raman scattering and chemical etching for layer removal appears as a very promising way to study the depth profile of the implantation damage. Recently, Holtz *et al.*[7] have employed this method to study low-energy (45-keV Be^+), ion-implanted GaAs. In the first part of the present work we use a similar approach, where Raman scattering combined with chemical etching is used to monitor the depth profile of the disorder created by 1-MeV Si implantation into GaAs, for fluences ranging from 1×10^{13} to 3×10^{15} cm^{-2}.

In perfectly crystalline semiconductors, the long-range periodicity of the lattice makes the correlation length of the normal-mode vibrations infinite, giving rise to the momentum selection rule, which limits Raman scattering to zone-center ($q=0$) optical phonon modes. Furthermore, symmetry-related selection rules allow or forbid the participation of these modes in the scattering process. As a result, the first-order Raman spectrum of a perfect crystal consists of one or more narrow peaks corresponding to the Γ point in the Brillouin zone. When defects are introduced in the lattice, for example, by ion implantation, the translational order of the lattice is disrupted and the correlation

[a] Analytical Technology Division.

 0021-8979/89/203515-08$02.40

length of the vibrational modes becomes finite. Such modes are no longer characterized by a single wave vector, and the momentum selection rule is relaxed. In the first-order Raman spectrum of an imperfect crystal the peaks of normally allowed modes appear broadened and shifted and, in addition, normally forbidden modes may become Raman active. In the limiting case of amorphous materials, translational symmetry is completely lost; the correlation length is of the order of the nearest-neighbor distance, and reciprocally, all the values of q are permitted in the Raman scattering process. All the phonons in the Brillouin zone contribute to the first-order spectrum of an amorphous sample, which resembles the one-phonon density of states of the crystal.[8] The intermediate state, that of partial disorder, is the most difficult to treat theoretically. To our knowledge no theory is available yet to describe the propagation of optical phonons in partially disordered crystals and to establish a relationship between specific lattice defects and Raman spectral features. A successful phenomenological model was developed by Richter, Wang, and Ley[9] to describe the Raman spectrum of polycrystalline silicon. They addressed the reduction in coherence length by imposing a Gaussian envelope of width $\sqrt{\ln 2}L$ on the phonon wave functions. This confinement leads to a range $\Delta q \sim 1/L$ of allowed phonon q values. Taking into account the extended range of the Raman-active phonons, they were able to account for the experimentally observed variations in the spectra of microcrystalline silicon. Moreover, they showed that the values of the parameter L used in their calculations were in good agreement with the dimensions of the crystallites determined by TEM. Later on Tiong *et al.*[6] used a model based on that of Richter and coworkers,[9] known today as the "spatial correlation (SC) model," to explain the Raman spectrum of ion-implanted GaAs. Here the parameter L had the meaning of an average undamaged region size.

In the second part of the paper we address the problem of the assignment of spectral features to particular lattice defects or structural modifications. We use the complementary information provided by ion-channeling measurements and TEM to obtain a detailed structural characterization of our MeV ion-implanted samples. We then compare the results of this characterization with some of the assumptions usually made to explain the Raman spectra of ion-implanted materials. In particular we show that the SC model provides a good fit to our experimental data, although we cannot find any evident correlation between the coherence-length parameter L used in the model and any defect-related characteristic length of the ion-implanted GaAs, thus casting doubts about the quantitative predictions of the model. We also show that the Raman spectrum of the MeV-implanted samples exhibits the characteristic bands resembling the one-phonon density of states of GaAs, which are usually attributed to amorphicity, although the TEM analysis showed no traces of amorphous material in our samples.

II. EXPERIMENT

Semi-insulating ⟨100⟩ GaAs samples were implanted in a nonchanneling direction with 1-MeV Si ions, using fluences ranging from 1×10^{13} to 3×10^{15} cm^{-2}. The beam current density was limited to $\sim0.5\,\mu$A/cm^2 to reduce beam heating effects. We have determined experimentally that, under this condition, the temperature of the samples does not rise more than 20–30 °C during the implantation. The chemical etching for depth profiling was performed using a solution of 50:3:3:CH_3OH:H_3PO_4:H_2O_2. The etch rate was calibrated using secondary-ion mass spectrometry to measure the shift of the Al signal before and after the etching steps in a sample consisting of 1 μm of GaAs epitaxially grown on AlGaAs. The etch rate of a sample implanted with 1×10^{15} Si/cm^2, at 1 MeV, was determined using secondary-ion mass spectroscopy to measure the shift of the Si depth profile after successive etch steps. The etch rate of GaAs was found to be 1200 ± 100 Å/min. The etch rate of the implanted sample was slightly slower, but within experimental error, than that of unimplanted GaAs. Thus the same etch rate was assumed for all samples used in the present study. Raman experiments were carried out at room temperature, in backscattering geometry, using the 514.5-nm line of a cw argon-ion laser. The scattered radiation was analyzed using a standard double-grating spectrometer in photon counting mode. The instrumental resolution was ~5 cm^{-1}. No polarization analyzer was used. The ion-channeling experiments were performed using 2-MeV $^4He^{++}$, typically with a current of 5–10 nA through a 1.5-mm-diam aperture. Backscattered particles were detected at a scattering angle of $\sim182°$ by a surface-barrier detector with energy resolution of <20 keV full width at half maximum. Samples for cross-sectional TEM (XTEM) were prepared by polishing and dimpling followed by Ar-ion thinning at liquid-nitrogen temperature to reduce ion-milling damage. Observations were made in a JEOL 2000FX instrument operating at 200 keV.

III. RESULTS

A. Raman spectroscopy

As a reference we present in Fig. 1 the Raman spectra of crystalline and amorphous GaAs in the energy-shift region ranging from 200 to 325 cm^{-1}. The crystalline spectrum (a), which corresponds to an unimplanted sample, is characterized by a narrow peak at 292 cm^{-1} arising from the zone-center longitudinal optical (LO) phonon mode. A very weak peak is also observed at 269 cm^{-1} arising from the zone-center transverse optical (TO) phonon modes. This last peak is symmetry forbidden in our (100) backscattering geometry. Its appearance is probably due to a small experimental deviation from true backscattering geometry or to some residual disorder on the surface of the sample. The amorphous spectrum (b), which corresponds to a sample rendered amorphous by implantation with 1 MeV, 1×10^{16} Si/cm^2, at liquid-nitrogen temperature, is characterized by a broadband centered at about 245 cm^{-1} (in the full spectrum there are two more broadbands at about 70 and 180 cm^{-1}, respectively) arising from the one-phonon density of states of GaAs.

Figure 2 shows the Raman spectra of GaAs implanted with 1-MeV Si ions, for fluences of 3×10^{13}, 3×10^{14}, and 3×10^{15} cm^{-2}. The spectrum of an unimplanted sample is

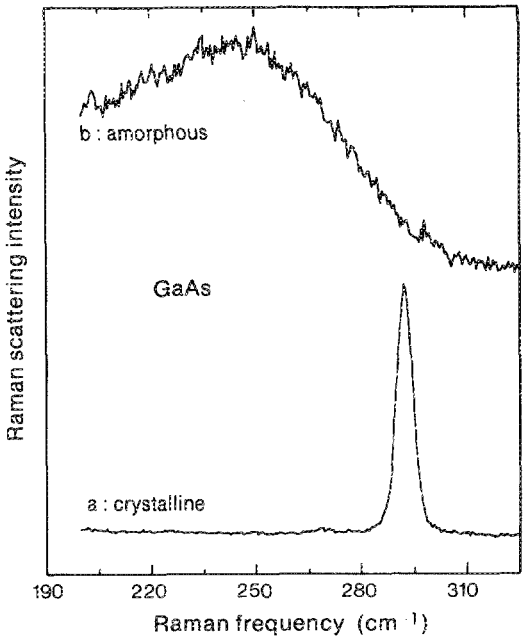

FIG. 1. First-order Raman spectra of (a) crystalline and (b) amorphous GaAs in the region 200–325 cm^{-1}. The amorphous spectrum (b) corresponds to a sample rendered amorphous (≈ 1 μm layer) by implantation with 1-MeV Si ions, to a fluence of 1×10^{16} cm^{-2}, at liquid-nitrogen temperature.

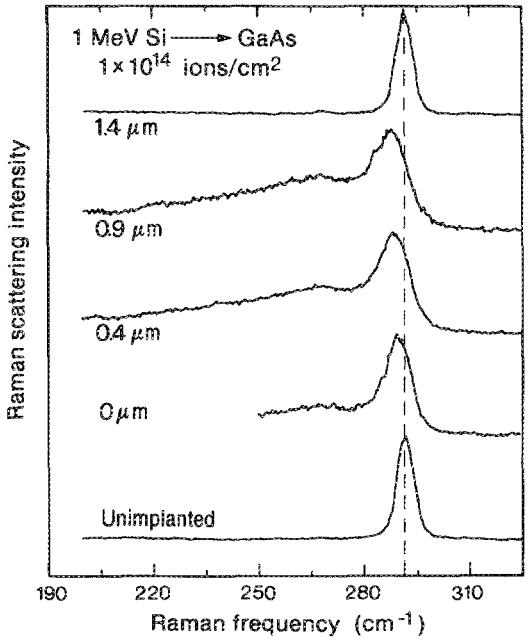

FIG. 3. First-order Raman spectra of GaAs implanted with 1-MeV Si ions to a fluence of 1×10^{14} cm^{-2}, taken on the original surface of the sample and after etching away 0.4, 0.9, and 1.4 μm, respectively. The spectrum of an unimplanted, not etched sample, is shown for reference.

also shown for comparison. The implants produce disorder in the GaAs lattice. This lattice disorder, in turn, induces changes in the Raman spectra. We observe that, with increasing implantation fluence, the LO line shifts to lower energies, broadens, and decreases in intensity. The TO line grows with increasing fluence and also broadens and shifts to lower energies. However, the downshift of the TO Raman line is much smaller than the downshift of the LO line. We also observe a long tail on the low-energy side of the TO line, which also grows in intensity with increasing implantation fluence.

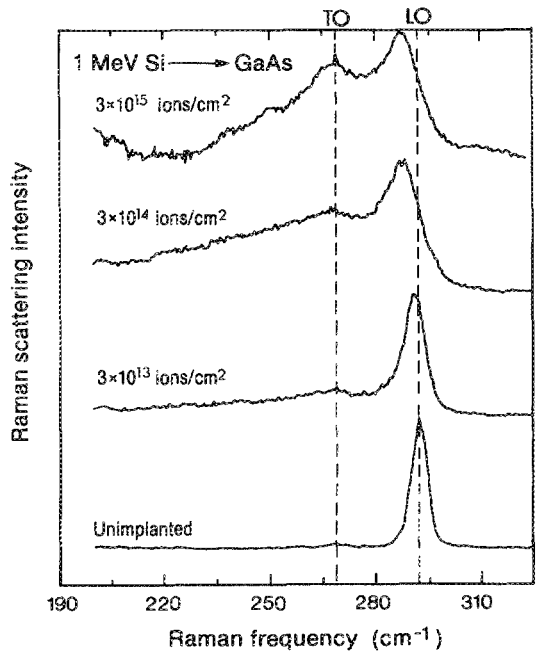

FIG. 2. First-order Raman spectra of crystalline GaAs and GaAs implanted with 1-MeV Si ions to fluences of 3×10^{13}, 3×10^{14}, and 3×10^{15} cm^{-2}. These spectra were taken on the original surfaces of the samples.

In Fig. 3 we present the Raman spectra of a sample implanted with 1×10^{14} Si/cm^2 at 1 MeV, taken at the surface of the sample and after etching 4000, 9000, and 14 000 Å, respectively. The LO peak shifts to lower energies, broadens, and decreases in intensity with increasing depth, from the surface down to 9000 Å. However, after 14 000 Å are removed, the LO line becomes narrow again and returns almost to the energy shift corresponding to unimplanted GaAs. The intensity of the TO mode increases, the peak broadens and shifts down in energy, with increasing depth from the surface down to 9000 Å. The TO peak has a long tail towards the low-energy region, which also grows with increasing depth. This tail results from the overlap of the TO line and the broadband centered at about 245 cm^{-1}, which was observed in the amorphous sample. After 14 000 Å are etched away the TO line becomes narrow and weak, returns to the position corresponding to pristine GaAs, and the low-energy wing disappears.

From the different features of the first-order Raman spectrum of GaAs, the position of the LO line appears to be most sensitive to the lattice disorder. Therefore, we use these changes to provide a qualitative description of the implantation damage. At this stage we do not attempt to identify the specific defects responsible for the LO shifts nor to use a more comprehensive model taking into account all of the features of the spectrum. In Fig. 4 we have plotted the frequency shift of the LO mode as a function of depth for a GaAs sample implanted with 1-MeV Si ions to the fluences

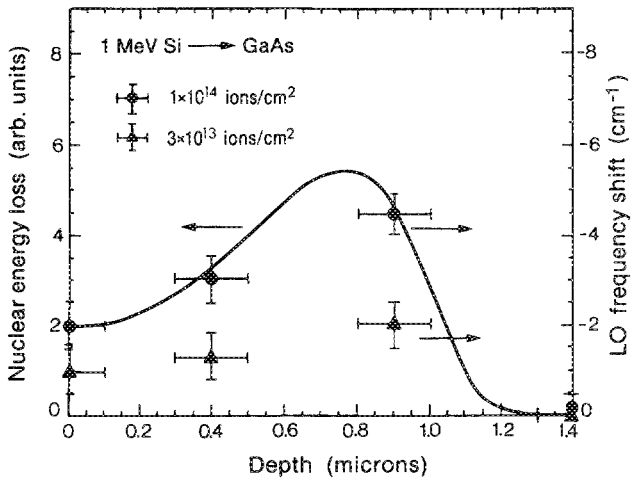

FIG. 4. LO-phonon frequency shifts, after various etch steps, for 1-MeV Si implanted into GaAs at fluences of ● 1×10^{14} cm^{-2}, and ▲ 3×10^{13} cm^{-2} compared to the depth profile of nuclear energy loss (i.e., radiation-damage depth profile) calculated using TRIM (Ref. 10) (solid line).

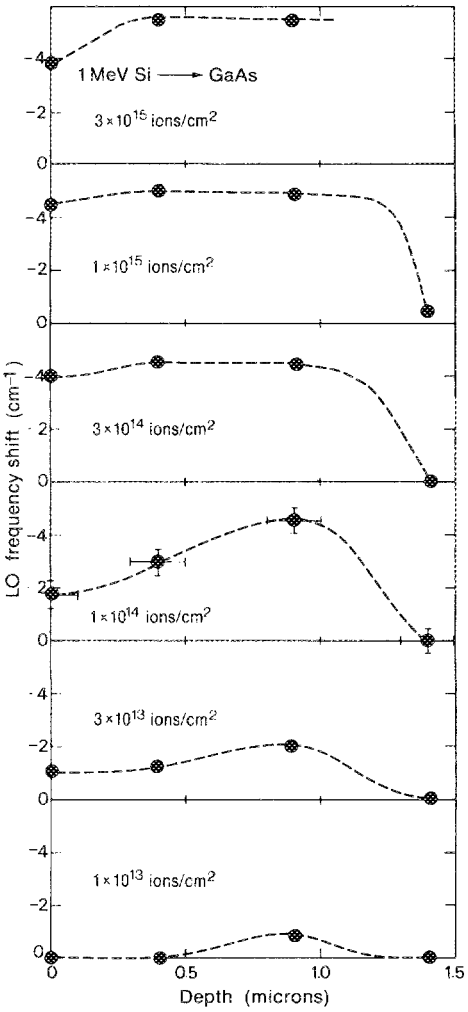

FIG. 5. Implantation-damage depth profile as a function of fluence for 1-MeV Si ions implanted into GaAs. The implantation damage is assumed proportional to the LO-phonon frequency shift as discussed in the text. The lines are only guides to the eye.

of 3×10^{13} and 1×10^{14} cm^{-2}. In the same figure and using the same depth scale, we have plotted the nuclear energy loss of the implanted ions. This energy loss, which results in the creation of lattice disorder, was calculated using the code TRIM.[10] It is evident that the LO shifts follow the nuclear-energy-loss curve. This observation has two important implications: First, the shifts in the LO energy provide a good gauge, qualitative at least, of the lattice disorder, and second, if indeed this is the case, the depth profile of the radiation damage in MeV implantations is closely related to the nuclear energy loss. The electronic energy loss, which corresponds to the energy going into excitation of electrons in the crystal, seems to play only a secondary role in the depth profile of the implantation damage. Having shown that the position of the LO line can be used as signature for the implantation damage, we plot in Fig. 5 the LO shift as a function of depth for samples of GaAs implanted with 1-MeV Si ions to fluences ranging from 1×10^{13} to 1×10^{15} cm^{-2}. At a fluence of 1×10^{13} cm^{-2} disorder starts to accumulate in a region starting at about 0.4 μm and ending at about 1.2 μm. The disorder in this region increases gradually as the fluence is increased to 3×10^{13} cm^{-2} and then to 1×10^{14} cm^{-2}. The disorder profile peaks at approximately 0.85 ± 0.1 μm. At these fluences disorder also starts to build up in the near-surface region of the sample. For fluences of 3×10^{14} cm^{-2} and higher, the disorder profile can be divided into three regions. In the central region, from about 0.3 to about 1.2–1.3 μm, the disorder approaches a saturation level characterized by an LO downshift of $5.0+0.5$ cm^{-1}. In the near-surface region, extending from the surface to a depth of about 0.3 μm, the amount of disorder is slightly smaller than in the central plateau. In the third and deepest region the structure changes gradually from a highly damaged material, at a depth of about 1.2 μm, to a nearly perfect crystal beyond 1.4 μm.

The preceding description of the evolution of the disorder profile with increasing fluence in MeV implantations is qualitatively similar to the description of the evolution of damage in low-energy implantations. The lattice disorder starts to build up at a depth slightly smaller than the projected range (R_p) of the implants. With increasing dose all the region, from the surface down to beyond R_p, becomes disordered. Only the saturation effect observed in high-energy implantations appears to be more pronounced than that observed in the low-energy case.[11] Both Raman spectroscopy and RBS-channeling analysis[12] show that the residual defects in 1-MeV implantation of Si into GaAs reach a maximum saturation value for fluences of the order of 5×10^{14}–1×10^{15} cm^{-2}. A similar effect was reported by Wie, Tombrello, and Vreeland,[13] who used x-ray rocking-curve measurements to determine the strain induced in GaAs by MeV implantation. They found that the strain perpendicular to the (100) GaAs surface saturated at a value of $\sim0.4\%$ for fluences in the range 1×10^{14}–1×10^{15} cm^{-2} (depending on the mass and energy of the bombarding ions). This saturation of residual disorder indicates that two competing processes are taking place simultaneously during high-energy implantations. Defects are created as a result of the atomic collisions that occur when the bombarding ions are slowed

down in the GaAs lattice. As shown in Fig. 4, the defect profile is closely related to the nuclear-energy-loss depth profile. However, the primary defects (vacancies and interstitials) are able to migrate and recombine or agglomerate, giving rise to the self-annealing process, which leads to the saturation of the residual disorder. The electronic energy loss was proposed in Ref. 12 as responsible for the defect recovery. In a separate paper[14] we have recently suggested that the dynamic annealing takes place using kinetic energy from the displacement cascade process, and therefore is primarily due to the nuclear energy loss.

In order to correlate the changes observed in the Raman spectra with structural changes in the ion-implanted samples, we find it necessary to provide a better characterization of the residual disorder. To this end we have carried out RBS-channeling and TEM studies of the implantation-induced damage, which we describe below.

B. RBS channeling

In Fig. 6 we present the aligned RBS-channeling spectra of GaAs samples implanted with 1-MeV Si ions using fluences of 3×10^{13}, 1×10^{14}, 3×10^{14}, 1×10^{15}, and 5×10^{15} cm^{-2} as well as the aligned and random (nonchanneling direction) spectra of an unimplanted sample. The energy of the backscattered particles has been translated into a corresponding depth of the scattering collision, and the resulting depth scale (based on the As signal) is also plotted in the upper margin of the figure. We observe an increase in the backscattering yield with increasing implantation fluence, but all the spectra show similar features as a function of depth. In each spectrum of the implanted samples, the yield gradually increases with increasing depth, from the surface to about 1.3 μm, reflecting the presence of residual defects in the lattice. At about 1.3 μm (slightly different for each sample) there is a change in the slope (yield versus depth) of the aligned spectra which becomes smaller, approaching the value of the unimplanted sample. This deeper region corresponds to the undamaged portion of the samples.

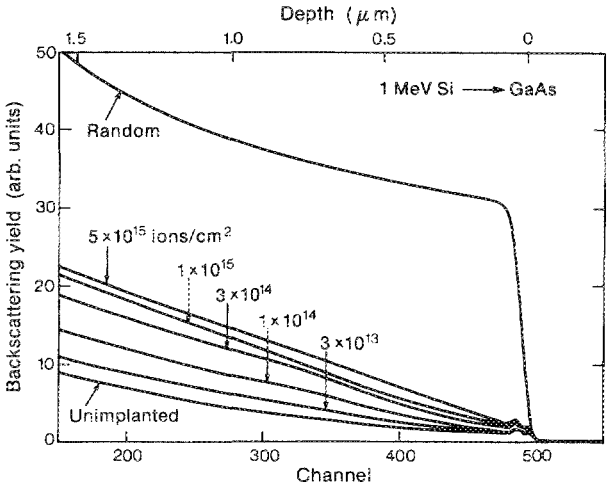

FIG. 6. Aligned RBS-channeling spectra of GaAs implanted with various fluences of 1-MeV Si ions. The aligned and random spectra of the unimplanted GaAs are also shown.

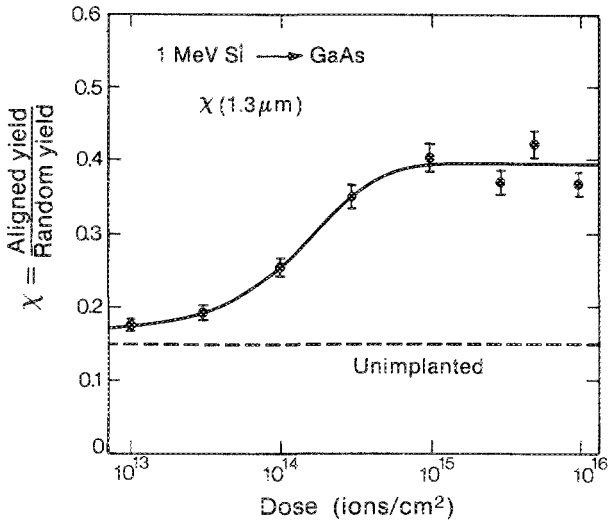

FIG. 7. Normalized backscattering yield χ (χ = aligned yield/random yield) as a function of implantation fluence in 1-MeV Si-implanted GaAs. χ was evaluated just beneath the disordered region at a depth of 1.3 μm and provides a qualitative estimate for the implantation-induced lattice damage.

A qualitative but convenient way to characterize the level of disorder in ion-channeling studies is by means of the normalized backscattering yield χ, defined as the aligned yield divided by the random yield at a given depth. We have plotted in Fig. 7 the normalized yield χ measured at about 1.3 μm as a function of implantation dose. We observe that χ increases with increasing fluence from 1×10^{13} to about 1×10^{15} cm^{-2} and then saturates. This plateau in the curve is a manifestation of the *in situ* annealing described in the previous section. The fact that most of the probing beam can traverse the disordered region, without losing the channeling alignment, indicates that the overall crystalline structure has not been destroyed, but rather locally disturbed by the implantation. In channeling analysis a gradual increase of the backscattering yield as a function of depth is attributed to defects that distort but do not block the channels, like dislocations, for example, or to a low concentration of interstitial point defects.[15]

C. TEM

Additional information about the structure of the ion-implanted samples was obtained using TEM. Figure 8 shows a cross-section micrograph of a sample implanted with 1-MeV Si ions to a fluence of 3×10^{15} cm^{-2}. Small, spotlike defects can be seen to extend from the surface down to a depth of 1.3 μm. Under high-resolution imaging conditions, the spotlike defects were identified as interstitial dislocations lying in the {111} planes which, viewed edge on, have diameters that range from 30 to 80 Å (Fig. 9). The extra plane of atoms in the core of the dislocation loop distorts the surrounding lattice giving rise to the half-moon shaped contrast regions on either side of the dislocations. The size of the contrast blobs can be used to assess, approximately, the dimension of the strained region surrounding each loop. Inspection of Fig. 9 reveals that the radii of the strained volumes are similar to the radii of the respective dislocation

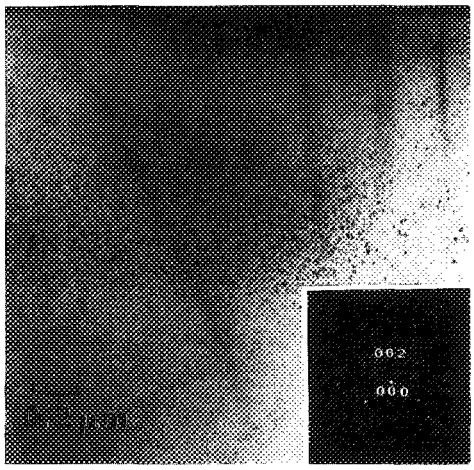

FIG. 8. Cross-section TEM micrograph showing the depth distribution of implantation-induced defects in GaAs implanted with 1-MeV Si ions to a fluence of 3×10^{15} cm^{-2}. The inset is a selected-area diffraction (SAD) pattern from the highest defect density region. The sharp SAD spots and the absence of diffraction rings indicate that the crystallinity of the lattice is highly preserved.

loops and thus range from 15 to 40 Å. Attempts to determine the crystallinity of the implanted region were made by using select-area diffraction (see inset of Fig. 8), convergent-beam electron diffraction (using 80-Å-diam beam size), and high-resolution lattice imaging. Except for the lattice disorder in the core of the dislocations, no evidence of any significant size amorphous areas was found. Indeed, the implantation-induced defects appear to consist of individual dislocation loops surrounded by an otherwise perfect lattice structure. Considering the limitation of the TEM and the techniques used, only point defects and small amorphous regions (<5 Å) would remain undetectable in the present study.

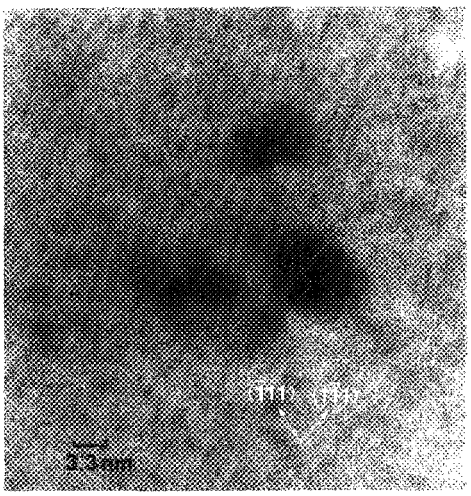

FIG. 9. High-resolution TEM image taken from the highest defect density region in Fig. 8, revealing that the defects are dislocation loops lying in the {111} planes of GaAs. Note also that the loops are isolated from each other and surrounded by a perfectly crystalline lattice structure (implantation: 1 MeV Si, 3×10^{15} cm^{-2}).

IV. DISCUSSION

The RBS-channeling and TEM measurements, presented in this and previous works,[12,14,16] provide a detailed characterization of the defect structure induced by the MeV ion implantation of GaAs, which could be of great help in determining the physical origin for the changes observed in the Raman spectra of ion-irradiated GaAs. As a result of these studies, the following description of irradiation-induced structural changes emerges: Point defects created by the impinging ions are able to migrate during the implantation owing to the excess energy gained by the lattice from nuclear and to some extent electronic energy-loss processes. Most of those defects either recombine or coalesce to form dislocation loops. After implantation there are no indications of microcrystalline or amorphous regions, and the isolated residual defects are embedded in a highly preserved crystalline structure. Wie and co-workers,[13] in their x-ray rocking curve studies of MeV-implanted GaAs, also concluded that after implantation the crystalline structure was highly preserved, but with residual defects that produced a small, uniform, uniaxial, lattice expansion. We use now the physical characterization of the MeV-implanted GaAs to reexamine some of the models and assumptions commonly used to explain the Raman spectra of ion-implanted materials.

In Sec. III A we took the change in the position of the LO line as a gauge to monitor the radiation damage without making any specific assumption about the nature of the defects or structural changes that gave rise to those shifts. We also neglected other features of the Raman spectra that can be used as spectral signatures for structural properties. These other features of the Raman spectra, i.e., disorder-induced bands, intensities, linewidths, etc., ought to be taken into account in order to establish a sound correlation between structural properties and Raman spectral features. An increasingly accepted approach to describe Raman scattering in ion-implanted materials is the use of the "spatial correlation (SC) model"[6,9] described in the introduction section. Following the procedure described by Tiong *et al.*[6] we have plotted in Fig. 10, as a solid line, the relationship between the LO phonon-line shift $\Delta w_{\rm LO}$ and the linewidth Γ as a function of the correlation length L, predicted by the SC model for GaAs. Also shown are our experimental values of $\Delta w_{\rm LO}$ and Γ for various implantation fluences and probing depths. The agreement is quite satisfactory and supports the validity of the model. Only a few points, those with the larger $\Delta w_{\rm LO}$ shifts, are seen to deviate noticeably from the calculated curve. This deviation can be accounted for if we take into account the strain-induced shift of the phonon lines.[17] A shift of 0.55 cm^{-1} was estimated in a Raman study[18] on samples similar to those used by Wie and co-workers and to our most damaged samples.

Since the SC model could be used to obtain a good fit to our experimental measurements, we tried to look for a possible correlation between the parameter L and some characteristic distance in the ion-implanted samples. As stated previously, the lattice structure of those samples consists of isolated dislocation loops and point defects dispersed in a perfectly crystalline material. The defect density is low enough that we cannot consider the original crystal broken

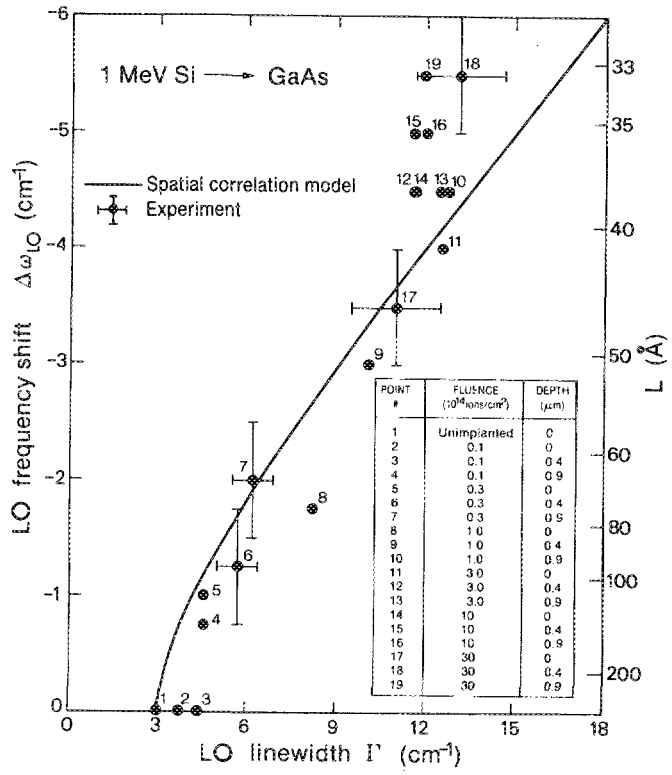

FIG. 10. Correspondence between the LO-phonon frequency shift and the LO linewidth in 1-MeV Si-implanted GaAs for various implantation fluences and etch depths. The solid line represents the correspondence predicted by the spatial correlation model (Refs. 6 and 9) In the right margin we have plotted the coherence-length parameter L used in the model, although in the text we show that there is no evident correlation between L and the average interdefect separation.

into a collection of smaller crystallites. We rather consider the crystalline order to be distorted in small, localized regions, which are distributed throughout the sample. Consequently, the only distance we can think of is the separation between the defects. We have estimated the separation between defects, for the sample implanted with 3×10^{15} Si/cm^2, in the buried region which shows the higher defect concentration. The separation between dislocation loops can be estimated from a TEM micrograph by counting the defects in a well-defined area and then establishing the thickness of the TEM specimen (in our case using thickness contrast contours). Following this procedure, we obtained a dislocation loop density $N_D \sim 8\times10^{16}$ cm^{-3}. If we assume that each defect is at the center of a cube with sides of length A, then the average separation between defects is also A and is given by $A = (1/N)^{1/3}$. In our case we obtained $A \sim 230$ Å. The determination of the separation between interstitials, which is done using the ion-channeling measurements, is less straightforward. The dechanneling yield in the ion-implanted crystals (see Fig. 6) is due in part to the interstitials and in part to the dislocation loops. The relative contribution of each type of defect to the dechanneling is extremely difficult to determine. Using standard dechanneling analysis methods,[15] we have estimated that if all the dechanneling in the sample implanted with 3×10^{15} cm^{-2} were due to interstitial point defects, their density in the buried defect band would be approximately 2.4×10^{21} cm^{-3}. This value sets an upper limit for the concentration of interstitials. However, in previous works[14,16] we have observed that after rapid thermal annealing of a similar sample, at 500 °C for 10 s, most of the point defects annealed out, whereas there was little change in the dislocation's density or size. Correspondingly, after annealing we observed a reduction in dechanneling yield to about one-half of the as-implanted value. We thus conclude that the interstitials account for approximately half the dechanneling yield in the as-implanted sample, and consequently, their concentration is estimated at $N_I \sim 1.2\times10^{21}$ cm^{-3}, which corresponds to $\sim$2.7% of the lattice atoms. The values of the average separation between dislocation loops and between interstitial point defects, along with the parameter L corresponding to this particular sample, are summarized in Table I. No evident correlation between the estimated interdefect distances and L is revealed in Table I. We are led to suggest that the correlation-length reduction, postulated in the SC model, is the result of the accumulative effect of phonon scattering by the lattice defects.

TABLE I. Comparison of the average separations between defects estimated from the RBS and TEM measurements and the correlation-length parameter L, predicted by the spatial correlation model (Ref. 10) for a sample of GaAs implanted with 1-MeV Si ions to a dose of 3×10^{15} cm^{-2}.

Average separation between dislocations	Average separation between interstitials	L
230 Å	9 Å	33.5 Å

Another significant finding of the present work is related to the identification of the structural disorder responsible for the broadband centered at about 245 cm^{-1}. This band, together with two more features appearing at 70 and 180 cm^{-1} but not covered in the present study, are broadened replicas of the one-phonon density of states of GaAs, which are usually considered to represent spectral signatures for amorphous GaAs. The TEM analysis could not detect any trace of amorphous region in any of our ion-implanted samples. However, the Raman spectra showed long tails on the low-energy sides of the TO peaks, clearly indicating the contribution of the 245-cm^{-1} band to the scattering yield. We conclude that the appearance of the 70-, 180-, and 245-cm^{-1} features is not necessarily due to amorphous regions in the sample (although the presence of amorphous material is a sufficient condition to induce these bands). Modest concentrations of defects in the lattice structure, most probably interstitial point defects, appear to disrupt the periodicity of the lattice enough to cause the relaxation of the momentum conservation rules, thus giving rise to the appearance of these bands.

In summary, we have determined the depth profile of implantation-induced lattice damage in 1-MeV Si-implanted GaAs using a combination of Raman scattering and chemical etching. The disorder depth profile, monitored through the changes in the LO-mode energy shift, agrees

qualitatively with the defect concentration profile predicted by TRIM.[10] However, with increasing implantation fluence, the amount of disorder reaches a saturation plateau indicative of the intense dynamical annealing that takes place during the high-energy implantations. The *in situ* recovery of the implantation damage is attributed mainly to the energy released to the lattice by nuclear-energy-loss processes. A detailed characterization of the implantation damage, carried out using ion channeling and TEM, showed that the residual disorder after implantation consists of dislocation loops and interstitial point defects dispersed in an otherwise perfect crystalline structure. An average separation between defects was estimated and compared with the coherence-length parameter L of the "spatial correlation model." Although the model provides a good fit to our data, in terms of the shift and broadening of the LO mode, no evident correlation could be found between L and the estimated interdefect distances. We suggest that the accumulative effect of phonon scattering by lattice imperfections is responsible for the reduction in the phonon's coherence length. We also showed that the broadbands appearing below 250 cm^{-1} are not necessarily due to amorphous GaAs, as is usually assumed.

Our results show that Raman scattering combined with chemical etching constitutes a rather simple and sensitive method to monitor the depth profile of implantation damage in MeV implantations, providing information complementary to that obtained by RBS or TEM. However, the quantitative interpretation of Raman spectra in terms of crystal quality, as well as the assignment of Raman spectral features to particular defect structures, requires further experimental understanding and therefore must be applied very cautiously in the present circumstances.

ACKNOWLEDGMENTS

We would like to thank Dr. G. Dresselhaus and Professor R. Zallen for their helpful advice, and J. Madathil and P. Fellinger for their technical help.

[1] M. D. Giles, in *VLSI Technology*, 2nd ed., edited by S. M. Sze (McGraw-Hill, New York, 1988), p. 327.
[2] N. W. Cheung, SPIE Proc. **530**, 3 (1985).
[3] See, for example, the bibliography section, L. C. Feldman, J. W. Mayer, and S. T. Picraux, *Materials Analysis by Ion Channeling* (Academic, New York, 1982), p. 235.
[4] R. Beserman, Acta Electron. **19**, 67 (1976).
[5] B. S. Elman, G. Braunstein, M. S. Dresselhaus, G. Dresselhaus, T. Venkatesan, and J. M. Gibson, Phys. Rev. B **29**, 4703 (1984).
[6] K. K. Tiong, P. M. Amirtharaj, F. H. Pollak, and D. E. Aspnes, Appl. Phys. Lett. **44**, 122 (1984).
[7] M. Holtz, R. Zallen, O. Brafman, and S. Matteson, Phys. Rev. B **37**, 4609 (1988).
[8] R. Shuker and R. W. Gammon, Phys. Rev. Lett. **25**, 222 (1970).
[9] H. Richter, Z. P. Wang, and L. Ley, Solid State Commun. **39**, 625 (1981).
[10] J. P. Biersack and L. G. Haggmark, Nucl. Instrum. Methods **174**, 257 (1980).
[11] J. S. Williams and M. W. Austin, Nucl. Instrum. Methods **168**, 307 (1980)
[12] S. T. Lee, G. Braunstein, and S. Chen, Mater. Res. Soc. Symp. Proc. **126**, 183 (1988).
[13] C. R. Wie, T. A. Tombrello, and T. Vreeland, Jr., Phys. Rev. B **33**, 4083 (1986).
[14] S. Chen, G. Braunstein, and S. T. Lee, Mater. Res. Soc. Symp. Proc. **138**, 233 (1989).
[15] L. C. Feldman, J. W. Mayer, and S. T. Picraux, *Materials Analysis by Ion Channeling* (Academic, New York, 1982), p. 117
[16] G. Braunstein, L. R. Zheng, S. Chen, S. T. Lee, D. L. Peterson, K. Y. Ko, and G. Rajeswaran, Mater. Res. Soc. Symp. Proc. (to be published).
[17] A. K. Sood, E. Anastassakis, and M. Cardona, Phys. Status Solidi B **129**, 505, (1985).
[18] G. Burns, F. H. Dacol, C. R. Wie, E. Burstein, and M. Cardona, Solid State Commun. **62**, 449 (1987).